RSC Advances

PAPER

View Article Online
View Journal | View Issue

Cite this: *RSC Adv.*, 2021, **11**, 2437

Lead-free bright blue light-emitting cesium halide nanocrystals by zinc doping†

Heng Xu, Jianghu Liang, Zhanfei Zhang, Zihao Deng, Yuankun Qiu, Maosheng He, Jianli Wang, Yajuan Yang and Chun-Chao Chen *

Received 15th November 2020
Accepted 28th December 2020

DOI: 10.1039/d0ra09705e

rsc.li/rsc-advances

Cesium lead halide perovskite nanocrystals (NCs) have attracted extensive attention for photoelectric device application due to their excellent optoelectronic properties. However, the toxicity of lead has hindered their commercialization. Consequently, lead free cesium metal halide NCs have been developed, but these materials suffer from low photoluminescence quantum yield (PLQY) and poor stability. Here, a new class of lead-free non-perovskite blue-emitting cesium bromine (CsBr) and cesium iodine (CsI) halide NCs are realized by zinc doping. High PLQYs of 79.05% and 78.95% are achieved by CsBr:Zn and CsI:Zn NCs, respectively, attributed to the improved local structural order and reduced strain between the lattices of the NCs after storing under ambient conditions for 20 to 30 days. Moreover, zinc doped cesium halide NCs show excellent air stability for at least 50 days. Our results for zinc doped cesium halide NCs have shown a new avenue to fabricate lead-free halide NCs for blue lighting and display applications.

Introduction

Recently, cesium lead halide ($CsPbX_3$, X = Cl, Br, I) nanocrystals (NCs) have attracted extensive research interest in devices such as solar cells,[1–5] light-emitting diodes (LEDs),[6–8] and photodetectors[9–11] and in laser[12,13] applications due to their superior photonic and electronic properties. Among these NCs, the perovskite lattice structure is commonly taken and contributes to their excellent optoelectronic properties. Although this new class of NCs based on halide perovskites are potential candidates for next generation lighting and display materials, scientists are still striving to improve their emission efficiency and air stability and, more importantly, reduce their toxicity. Currently, research progress on blue-emitting perovskite halide NCs is lagging behind that of green and red emitting perovskite halide NCs due to instability and low PLQY.[14–16] In particular, the replacement of the Pb cation in blue-emitting perovskite NCs to lower toxicity has sacrificed their PLQY significantly.[17] Hence, developing non-toxic lead-free blue-emitting NCs with high PLQY becomes an important task.[18–21]

Several low toxic metal cations have been used to fully or partially replace Pb in halide perovskite NCs, such as manganese (Mn),[22–25] nickel (Ni),[26,27] copper (Cu),[28–30] tin (Sn),[31–36] europium (Eu),[37] bismuth (Bi)[38–41] and zinc (Zn).[42–44] Mn was used to partially replace Pb to prepare less toxic $CsPb_{0.73}Mn_{0.27}Cl_3$ NCs with dual-color emission and greatly enhanced the PLQY of $CsPbCl_3$ from 5% to 54%.[25] Violet-emitting perovskite NCs with high PLQY of 96.5% were successfully synthesized by doping 11.9% molar ratio of Ni into $CsPbCl_3$ NCs.[26] $Cs_3Cu_2I_5$ NCs with a PLQY of 87% were prepared to fabricate high efficiency deep blue LEDs.[30] Furthermore, Sn was used to prepared $CsSnX_3$ NCs. However, only a low PLQY below 1% and poor air stability was found due to the fact that Sn^{2+} can be easily oxidized into Sn^{4+}.[33] The ionic radii of Eu^{2+} and Pb^{2+} are similar, so Eu has great potential to replace Pb. Blue-emitting $CsEuCl_3$ NCs with a PLQY of 5.7% was synthesized.[37] Bi was also introduced into perovskite NCs to prepare $Cs_3Bi_2Br_9$ NCs, which exhibit a blue emission with a PLQY of 4.5%.[38] Environmental friendly Zn was also used to replace Pb to prepare lead free halide NCs. Recently, blue-emitting Cu doped Cs_2ZnBr_4 NCs were prepared with a PLQY of 65.3%.[43] As a result, the replacement of Pb cation in blue-emitting halide perovskite NCs with a satisfactory PLQY continues to be an important task for researchers.

Besides halide perovskite NCs, the replacement of Pb in cesium lead halide NCs can sometimes lead to non-perovskite lattice structures, existing as doped cesium halide NCs, which are rarely studied. Cesium halides (CsX, X = Cl, Br, I) are wide bandgap materials used for scintillators due to their ability to absorb high-energy X-ray and turn into ultraviolet emission for X-ray detection.[45] In the commercially used CsX bulk crystals, Tl and Na doping are commonly applied to improve the emission performance of scintillators. However, their optical properties on the nanoscale have been rarely investigated up to date.[46–48] By introducing intermediate trap states *via* doping, Yang *et al.*

School of Materials Science and Engineering, Shanghai Jiao Tong University, Shanghai 200240, P. R. China. E-mail: c3chen@sjtu.edu.cn

† Electronic supplementary information (ESI) available. See DOI: 10.1039/d0ra09705e

reported the blue-emitting Eu^{2+} doped CsBr NCs with a PLQY of 32.8%.[49] Nevertheless, rare earth element Eu is limited due to its scarcity and high cost. Based on these preliminary results, more efforts are urgently required to study CsX NCs owing to their great potential in blue emission and non-toxic applications.

In this work, a new class of lead-free blue-emitting cesium halide NCs is developed by introducing Zn as doping cation into the lattice of CsBr and CsI. The zinc doped cesium halide (CsBr:Zn and CsI:Zn) NCs synthesized *via* modified hot injection method are found to exhibit a cubic structure, instead of perovskite structure. Furthermore, we observe the self-growing process of CsBr:Zn NCs with gradually improved local structure order and reduced strain when precipitating the particles and re-dispersing them in a clean solvent for 30 days. As a result, significantly high PLQY of 79.05% and 78.95% are measured for CsBr:Zn and CsI:Zn NCs, respectively. To the best of our knowledge, the high PLQY of these NCs materials prepared in our work are comparable with the best of $CsPb(Br_{1-x}Cl_x)_3$ perovskite quantum dots,[50] carbon dots,[51] commercial Cd-based quantum dots[52] and other lead-free halide NCs in blue-emitting region (Table S1†). The demonstration of zinc doped cesium halide NCs *via* modified hot injection method has introduced a new class of lead-free blue-emitting cesium metal halide NCs for future lighting and display applications.

Experimental

Chemicals

Cesium carbonate (Cs_2CO_3, 99% metals basis), octadecene (ODE, technical grade, 90%), oleic acid (OA, 85%), oleylamine (OLAM, 80–90%), and hexane (analytical grade) were purchased from Aladdin. Zinc bromide ($ZnBr_2$, 99.9% metals basis) and zinc iodide (ZnI_2, analytical grade, 98%) were purchased from Macklin. Silica gel (ET-821 A and B) used for LED package was purchased from IED Technologies Co. Ltd. All chemicals were used without further purification.

Preparation of cesium oleate as a cesium precursor

Cs_2CO_3 (0.540 g, 1.6574 mmol), ODE (20 mL) and OA (1.9 mL) were loaded into a 50 mL 3-neck round bottom flask, dried for 30 minutes at 120 °C, and then kept at 100 °C under N_2 until all Cs_2CO_3 reacted with OA.

Synthesis of zinc doped cesium halide nanocrystals

ODE (30 mL), OA (0.36 mL), OLAM (3 mL) and $ZnBr_2$ (0.540 g, 2.3979 mmol) were added to a 100 mL 3-neck round bottom flask and kept at 120 °C under N_2 until all $ZnBr_2$ was completely dissolved. Then the reaction was kept at 160 °C under N_2 for 10 minutes and cesium oleate solution (4.5 mL, prepared as described above) was quickly injected. 2 minutes later, the reaction mixture was cooled by ice-water bath with continuous stirring for 1 minute. The ice-water cooled crude solution was purified *via* a high speed centrifuged (at 8000 rpm for 5 minutes). After centrifugation, the supernatant was discarded and the particles were re-dispersed in hexane. For the synthesis of other zinc doped cesium halide NCs, $ZnBr_2$ was simply replaced by ZnI_2.

Fabrication of the blue LED

The prepared CsBr:Zn NCs solution was added into the mixture of silica gel ET-821 A and B, and stirred for 15 minutes for fully mixing CsBr:Zn NCs and silica gel. The obtained mixture was put into an oven at 40 °C for 15 min to evaporate the solvent. Then it was coated onto the LED chip.

Characterization

X-ray diffraction (XRD) spectra were measured with a Bruker-D8 Advance using Cu Kα radiation (λ = 1.5406 Å) at room temperature by drop-casting CsBr:Zn NCs solution on a glass and heating at 120 °C to remove the solvent. Transmission electron microscopy (TEM) and high-resolution TEM (HRTEM) images were acquired on a JEOL JEM-2100 electron microscope with an accelerating voltage of 200 kV by drop-casting NCs solution onto 300 mesh carbon-coated copper grids. Energy dispersive spectrometer (EDS) measurement was done with a TESCAN MIRA3 and Aztec X-MaxN80 instrument by drop-casting NCs solution onto a conductive silicon slide. X-ray photoelectron spectroscopy (XPS) measurement was carried out with an AXIS UltraDLD instrument by drop-casting NCs solution onto a glass slide. UV-visible absorption spectra of NCs solution were recorded by using a PerkinElmer Lambda35 spectrometer. Photoluminescence (PL) and PL excitation (PLE) spectra of NCs solution were performed on a PerkinElmer LS55 luminescence spectrometer. A quartz cuvette of 10 mm path length and volume 3 mL was used for collecting the spectra. Photoluminescence quantum yield (PLQY) absolute quantum yield and time-resolved PL (TRPL) decay curve measurement of NCs solution were carried out by a PTI QM/TM/IM steady-state and time-resolved fluorescence spectrometer. The PLQY was measured by using a Beckman integrating sphere with a diameter of 80 mm. We firstly placed a blank quartz plate in the integrating sphere to measure the reference. Then we measured the emission spectrum of the sample excited by 360 nm light in the integrating sphere as well. *Via* calculation of emission divided by absorbance, the PLQY of the sample was obtained at room temperature. The time-resolved PL decay spectrum was measured with an excitation from the pulse laser of 380 nm. The decay curve can be well fitted with a mono-exponential function: $I(t) = A\exp(-t/\tau)$, where τ represents the lifetime of the blue emission band, indicating only one emission center in the sample. TGA of NCs powder was recorded by Discovery TGA55 at a heating rate of 10 °C min^{-1} in the range of 20–900 °C under nitrogen flow. The LED properties were measured by an integrating sphere HAAS2000.

Results and discussion

Synthesis of CsBr:Zn NCs

The CsBr:Zn NCs were synthesized using a modified hot-injection method by injecting cesium oleate precursor into a solution of zinc bromide ($ZnBr_2$), oleic acid (OA), and

oleylamine (OLAM) in octadecene (ODE). An injection temperature of 160 °C is needed. During the synthesis process, by reducing the ratio of OA and increasing the amount of $ZnBr_2$, the highest PL intensity of the sample was achieved. By re-dispersing CsBr:Zn NCs in clean hexane and storing them for about 30 days at ambient condition, CsBr:Zn NCs in hexane show bright blue emission under UV-light irradiation, with a corresponding PLQY measured as high as 79.05%, which is comparable with the best blue-emitting quantum dots.[50–52]

The morphology of the prepared CsBr:Zn NCs (stored at ambient condition for 30 days) observed by transmission electron microscopy (TEM) is presented in Fig. 1a and b. It showed uniform morphology in hexagonal-shape with an average size diameter of 23.3 nm (Fig. 1a). A similar shape has been also reported in CsBr NCs[53] and CsBr:Eu^{2+} NCs.[49] High-resolution TEM (HRTEM) of CsBr:Zn NCs reveals that they are crystalline with no obvious crystal defects and that the lattice distance is 0.301 nm (Fig. 1b and S1†), corresponding to the (110) crystal facet of pure CsBr. The selected area electron diffraction (SAED) pattern in Fig. 1c also matches well to the crystalline nature of pure CsBr. X-ray diffraction (XRD) patterns of CsBr:Zn NCs were measured to verify the crystal structure in Fig. 1d, confirming that CsBr:Zn NCs are crystalline with cubic structure and hold *Pm3m* space group. The peak positions of CsBr:Zn NCs are coincident with the standard file (ICDD card no 050588). The dominant diffraction peaks are indexed at $2\theta = 29.56°$, 42.31° and 52.35°, corresponding to diffraction from the (110), (200), and (211) planes, respectively.[49,53] However, no diffraction of Zn, $ZnBr_2$ or other secondary phases were observed, as other reports referred.[54,55] It's worth to note that the calculated crystal parameter of CsBr:Zn ($a = b = c = 4.283$ Å, $\alpha = \beta = \gamma = 90°$) is slightly smaller than that of CsBr ($a = b = c = 4.296$ Å, $\alpha = \beta = \gamma = 90°$) due to the lattice distortion brought by the presence of divalent zinc in these crystals. Meanwhile, it is generally believed that doping smaller-sized cations (0.60 Å for Zn^{2+} ionic radii *vs.* 1.67 Å for Cs^{+}) would cause the contraction of cubic lattice. The contraction lattice of CsBr:Zn NCs can also be confirmed by higher angles shift of the XRD peaks.

To confirm that Zn is doped into CsBr NCs, energy dispersive spectrometer (EDS) measurement and X-ray photoelectron spectroscopy (XPS) measurement were carried out. The individual elemental maps of Cs, Br and Zn are illustrated in Fig. 2. Zn is evenly distributed throughout the field of the sample, as well as Cs and Br. The calculated percent composition of the constituent elements of CsBr:Zn NCs is 36.24% for Cs, 56.61% for Br, and 7.15% for Zn. Abundant Br does not only balance the charge of the system, but also reduce the surface traps and improve the PL performance of the NCs.[56–58] We further performed XPS measurement to study the surface chemistry of CsBr:Zn NCs (Fig. S2†). The Cs 3d spectrum exhibits two dominant peaks located at 723.9 and 737.8 eV, corresponding to the Cs 3d5/2 and Cs 3d3/2 level, respectively. The binding energy peaks of Br 3d at 68.0 eV (Br 3d5/2) and 68.9 eV (Br 3d3/2) are also observed in the Br 3d spectrum for the CsBr:Zn NCs. Meanwhile, the presence of Zn in the lattice has been further confirmed from Zn 2p spectrum, demonstrating two characteristic peaks located at 1021.7 eV for Zn 2p3/2 and 1044.7 eV for Zn 2p1/2 level. We also note that the peaks of C 1s, O 1s and N 1s can be obviously observed besides the peaks of Cs 3d, Br 3d and Zn 2p, which indicates that the CsBr:Zn NCs are surrounded and passivated by rich OA and OLAM ligands and may be a reason for their excellent properties. The result of XPS is consistent with the above EDS analysis, suggesting the successful doping of Zn into CsBr lattice.

Optical properties of CsBr:Zn NCs

The UV-visible absorption, photoluminescence (PL) and PL excitation (PLE) spectra of the sample are presented in Fig. 3a, and the inset picture shows photographs of colloidal CsBr:Zn NCs solution under room light and a 365 nm UV light excitation. CsBr:Zn NCs demonstrate a typical sharp absorption band at around 230 nm. And two weak bands at 381 nm and 404 nm in the tail are shown in the magnified view of bands in Fig. S3.† The absorption tail with two weak bands in the long wavelength region, which are not supposed to appear at a simple CsX NCs,[53] is attributed to the introduction of the additional intermediate

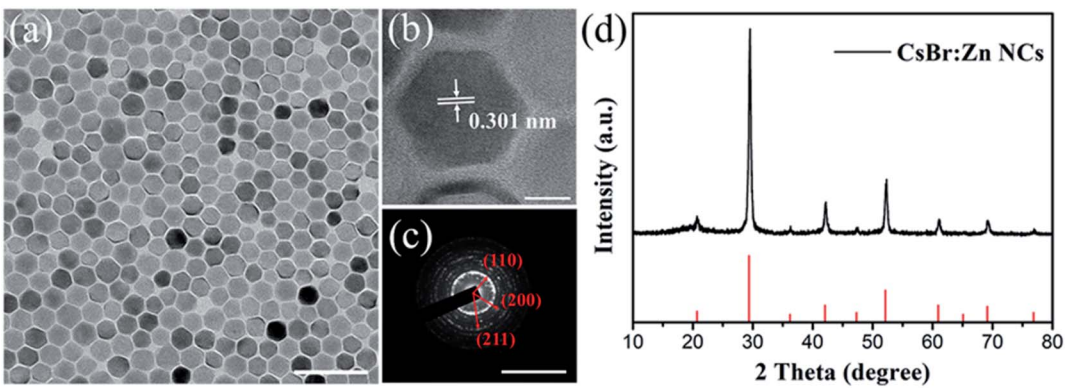

Fig. 1 (a) Transmission electron microscopy (TEM) image, (b) high-resolution TEM (HRTEM) image and (c) selected area electron diffraction (SAED) pattern of CsBr:Zn NCs. (d) XRD patterns (black line) of as-prepared CsBr:Zn NCs in comparison with the corresponding reference patterns (ICDD no 050588 for CsBr, red line). (Scale bar for (a) 100 nm, for (b) 10 nm and for (c) 10 1/nm).

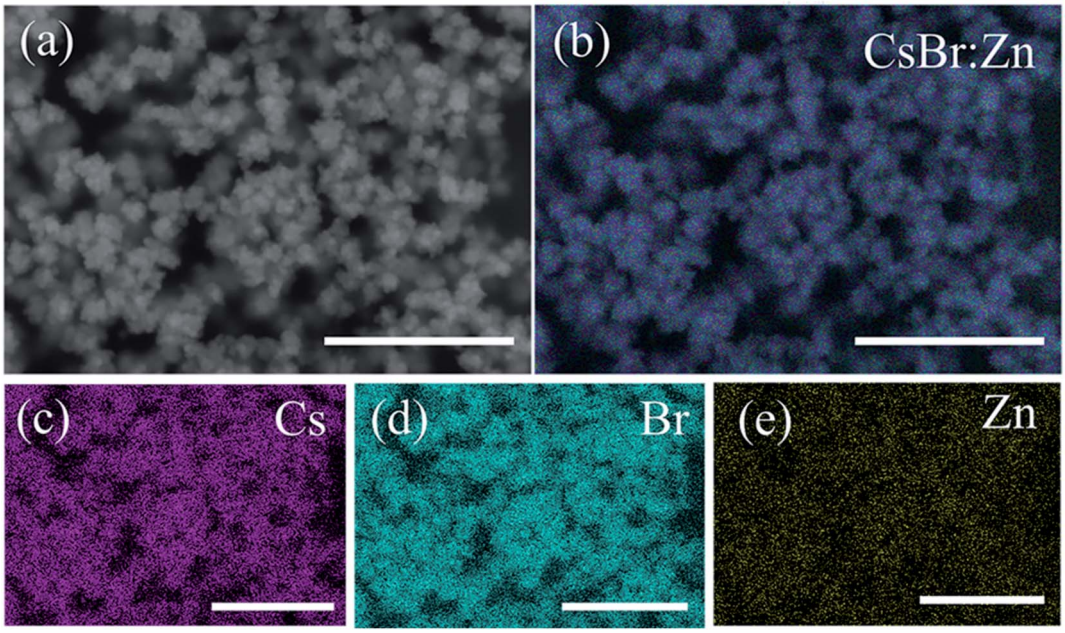

Fig. 2 Elemental characterization of CsBr:Zn NCs. (a) SEM image of CsBr:Zn NCs. (b) EDS mapping of CsBr:Zn NCs. (c–e) Corresponding elemental mapping of Cs, Br, and Zn in CsBr:Zn NCs. Scale bars are 5 μm in all images.

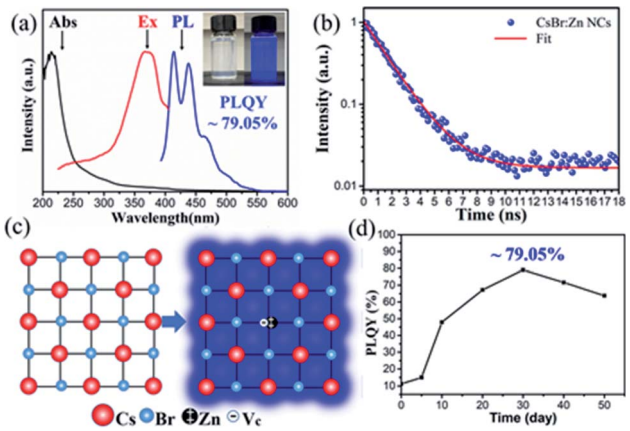

Fig. 3 (a) UV-visible absorption (black line), PL (blue line) and PLE (red line) spectra of CsBr:Zn NCs. Inset in the top right shows photographs of CsBr:Zn NCs solution under room light and a UV light excitation (365 nm). (b) Time-resolved PL decay and fitting curve of CsBr:Zn NCs. (c) The formation of the blue-emitting CsBr:Zn NCs, where a Cs^+ site is replaced by the combination of a Zn^{2+} and a vacancy (V_c^-) in CsBr crystal structure. (d) PLQY values of CsBr:Zn NCs over storage time at ambient condition.

trap states by Zn doping in original energy level, and correlated well with the emission peaks of CsBr:Zn NCs.

The emission spectra of the CsBr:Zn NCs is largely determined by Zn doping since CsBr NCs is originally non-emissive.[53] The PL spectrum of CsBr:Zn NCs under excitation at 380 nm consists of multi peaks, instead of a single peak, with a wide range from 395 nm to 550 nm. Two main peaks are centered at 415 nm and 438 nm in PL spectrum, respectively, which are in a good agreement to the two weak absorption band edges at 381 nm and 404 nm with a Stokes shift of 34 nm for each peak. The FWHM of CsBr:Zn NCs is 47 nm, comparable with other lead-free halide NCs. Based on 10 samples, we measured the PLQY of CsBr:Zn NCs with a value of 78.51 ± 0.54%. Notably, the CsBr:Zn NCs exhibit the brightest blue emission with the highest PLQY up to 79.05% (Fig. S4†). It needs to be emphasized that the 79.05% PLQY is among the highest one for lead-free halide NCs in the blue-emitting region. Yang *et al.* reported the nature of multiple and asymmetric bands of blue emission in CsBr:Ca^{2+} NCs is caused by the incorporation of Ca^{2+} ion.[49] Therefore, the luminescence of CsBr:Zn NCs can also originate from Zn^{2+} doping, which will be discussed later.

Besides, PLE spectrum of CsBr:Zn NCs exhibits a strong peak at around 370 nm. The constant shape of PLE spectra when varying the emission wavelength (Fig. S5a†) indicates that the multi PL peaks of CsBr:Zn NCs origin from the same energy recombination channel, *via* the luminescent centers introduced by zinc doping. Meanwhile, no obvious spectra shift in excitation-dependent PL spectra (Fig. S5b†) also shows that the multi blue emission peaks of CsBr:Zn NCs are caused by the relaxation of almost the same excited states. The results above show that the multiple blue-emitting peaks of CsBr:Zn NCs originate from the same luminescence mechanism, that is to say, the photons released by radiative recombination come from a specific way instead of multiple ways. The specific way of recombination can be related to the intermediate trap states introduced by Zn doping. The photophysical process in CsBr:Zn NCs is shown in Fig. S6.† In addition, the stable peak position together with high PLQY of CsBr:Zn NCs indicates their potential to be a good candidate for intense and stable light irradiation sources in blue region.

Fig. 3b shows the corresponding time-resolved PL (TRPL) decay curve of CsBr:Zn NCs with an excitation of 380 nm. The curve can be well fitted by mono-exponential decay behaviour ($R^2 = 0.995$), which also indicates a single pathway of radiative recombination with an extremely low defect density.[59,60] While the corresponding PL lifetime is as low as 1.63 ns, it is still of the same magnitude as that of $CsPbCl_3$ (ref. [17]) and Cs_2ZnCl_4 (ref. [44]) NCs. The obtained short-lived PL decay lifetime can be ascribed to exciton recombination. The mono-exponential fitting result offers reasonably agreement with the high PLQY of 79.05% of the CsBr:Zn NCs.[59] In addition, the PL intensity of CsBr:Zn NCs with a linear dependence of the excitation power indicates that the origin of photoemission is not permanent defects (Fig. S7†).[61] To further explore the luminescence mechanism of CsBr:Zn NCs, we tested the temperature dependent PL spectra from 80 K to 300 K (Fig. S8†). PL intensity increases with the increment of the temperature termed as negative thermal quenching,[62–64] which is quite anomalous for normal semiconductor NCs. Here, the domination of radiative relaxation process in CsBr:Zn NCs is evidenced because the nonradiative relaxation process will lead to thermal quenching, which means PL intensity decreases with the increasing temperature. The reason of this interesting behaviour may be explained considering the involvement of intermediate trap states introduced by zinc doping. At suitable temperature, the charge carriers captured by the intermediate trap states can be activated and released due to enough thermal energy, and transit to ground state followed by radiative recombination. Then, an increment of PL intensity is observed. However, the thermal energy is insufficient for releasing the carriers captured by intermediate trap states at lower temperature. It's worth to note that the temperature, which can provide enough energy, is as low as 120 K. Therefore, CsBr:Zn NCs show a bright blue emission at room temperature. The FWHMs of CsBr:Zn NCs increase as the temperature increases, which is consistent with other reports, because of more active lattice structure vibration at higher temperature.

Furthermore, many reports have shown that the impurity doping can bring new bands between the original conduction band minimum (CBM) and valence band maximum (VBM) of the host materials, and therefore greatly change their optical properties.[42,43,49,65,66] Here, both CsX (X = Br and I) are essentially insulators with large bandgaps. For example, CsBr has a bandgap of 4.2 eV. After Zn doping, CsBr:Zn NCs exhibit a bright blue emission of 415 nm and 438 nm under UV-light excitation, which essentially means that Zn doping introduces new bands with lower energy in the blue emitting region. Once again, we like to suggest that bandgap narrowing for CsBr:Zn NCs can be originated from the intermediate trap states introduced by Zn doping *via* its d–d transitions.[65] A recent report from Liao *et al.* suggests that upon impurity doping Zn^{2+} and other transition metal ions with similar electronic configuration (d^9–d^{10}) are capable of decreasing the bandgap of halide NCs *via* the overlapping of p orbitals of halide anions and d orbitals of Zn^{2+} cations in the valence band.[67] Moreover, in the lattice of CsBr:Zn NCs, the combination of a divalent Zn^{2+} cation and a vacancy (V_c^-) can replace a Cs^+ site in the monovalent CsBr host to keep the charge balance, as shown in Fig. 3c, which is commonly seen in the divalently-doped cesium halide crystals represented by Pb^{2+}, Sn^{2+} and Eu^{2+}.[68–70] The bright blue emission of CsBr:Zn NCs can take place from the exciton localized near Zn^{2+}–V_c^- pair. Further studies are ongoing to investigate the mechanism of Zn doping. The change in PLQYs of CsBr:Zn NCs over time is presented in Fig. 3d. The PLQY increases with storage time until a maximum of 79.05% is reached. In this case, CsBr:Zn NCs were stored at ambient condition for 30 days. Then the PLQY decreases and remains at 63.77% after 50 days. The result shows that CsBr:Zn NCs are stable under air condition for at least 50 days. To clarify this interesting observation, the structure and morphology of CsBr:Zn NCs related to storage time are discussed in the following part.

Structure–optical properties relationship of CsBr:Zn NCs

To clarify the structure–optical properties relationship between PLQY and storage time, we further measured the TEM images

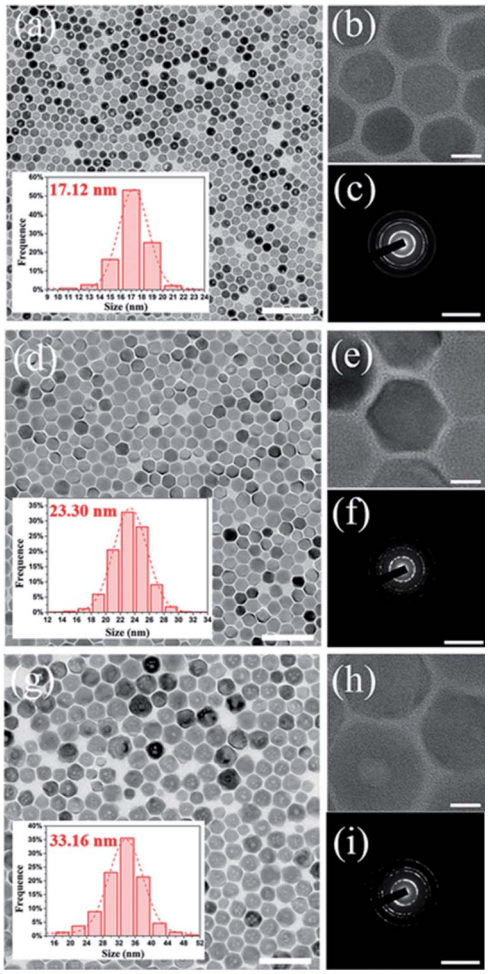

Fig. 4 TEM images, HRTEM images and SAED patterns of CsBr:Zn NCs after stored for 3 days (a–c), 30 days (d–f) and 50 days (g–i), respectively. Insets in TEM images are particle size statistical histograms of CsBr:Zn NCs at different storage time. Scale bars present 100 nm for (a), (d) and (g); 10 nm for (b), (e) and (h); 10 1/nm for (c), (f) and (i).

(Fig. 4) and XRD patterns (Fig. S9†) of CsBr:Zn NCs over time. In Fig. 4, the size and shape of CsBr:Zn NCs change with the storage time. The size of CsBr:Zn NCs becomes lager while storage time increases. The shape of CsBr:Zn NCs remains regular hexagonal-shape in 30 days, but partially changes into cubic-shape after stored for 50 days, which can be seen clearly in the HRTEM images. TEM diffraction patterns of CsBr:Zn NCs after stored for 3 days, 30 days and 50 days are similar, so the crystal structure of CsBr:Zn NCs is stable for a long term storage. This can also be confirmed by the unchanged XRD patterns at different days in nearly 2 months (Fig. S9†).

We calculate the size and strain of CsBr:Zn NCs from the XRD patterns, as shown in Table S2.† The calculated size of CsBr:Zn NCs at different days from XRD is in good agreement with the TEM result. It is worth to note that the calculated strain between CsBr:Zn NCs is so large at beginning, thus causing the originally weak photoluminescence of the fresh NCs. Then, the calculated strain for CsBr:Zn NCs decreases in the first 30 days, then slowly increases afterward. Again, it is worth to note that after 30 days the regular hexagonal CsBr:Zn NCs with a diameter of 23.3 nm have the lowest strain, corresponding to the minimum lattice distortion caused by the doping of Zn. The increased order of the lattice can be beneficial for the trapped photons produced by the radiative recombination to be effectively released from the lattice, contributing to the highest PLQY.[26] When the calculated strain slowly increases afterward, PLQY also decreases to 63.77%. From results above, the optical properties of CsBr:Zn NCs is dependent on their structural properties, such as morphology and strain. These findings indicate that the high PLQY and good air stability of CsBr:Zn NCs can be due to improved local structure order and less strain of the crystal during the self-growing process for first 30 days.

Stability of CsBr:Zn NCs

We also studied the stability of CsBr:Zn NCs. They are stable under air condition (relative humidity: 40–50%) for at least 2 months, as supported by the similar TRPL spectra of CsBr:Zn NCs at different temperatures and stored days (Fig. S10†) and the bright blue emission pictures for the 30th and 60th day under a 365 nm UV light (Fig. S11†). CsBr:Zn NCs also have good thermal stability, confirmed by the thermogravimetric analysis (TGA) measurement under nitrogen flow from 20 to 900 °C (Fig. S12†). A slight weight loss at around 250 °C can be attributed to the loss of organic ligands. A large weight loss of around 750 °C is due to the decomposition of CsBr:Zn NCs.[29]

Synthesis of CsI:Zn NCs

In addition, the synthesis method can be applied to other zinc doped cesium halide NCs by using ZnI_2 salt as precursor. As show in Fig. 5, blue-emitting CsI:Zn NCs were also prepared (stored at ambient condition for 20 days). The PLQY of CsI:Zn NCs was measured to be 78.32 ± 0.63% based on 10 samples, with the highest PLQY of 78.95% (Fig. S13†). Compared with CsBr:Zn NCs, the shape of CsI:Zn NCs changes to quasi-spherical with an average diameter of 18.11 nm, as shown in Fig. 5a. HRTEM images (Fig. 5b) of CsI:Zn NCs shows a lattice

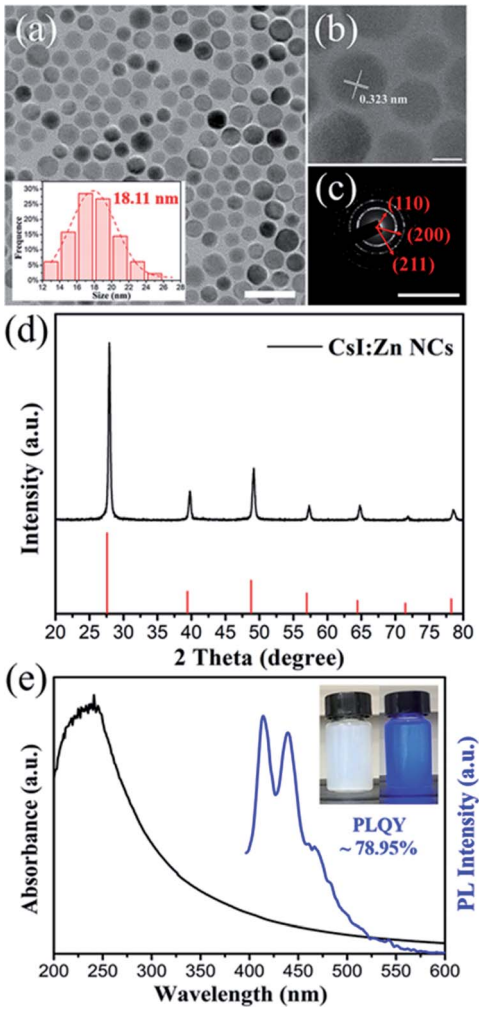

Fig. 5 (a) TEM image, (b) HRTEM image and (c) SAED pattern of CsI:Zn NCs. Inset in TEM image presents particle size statistical histogram of CsI:Zn NCs. Scale bar for (a) is 50 nm, for (b) is 10 nm and for (c) is 10 1/nm. (d) XRD patterns (black line) of as-prepared CsI:Zn NCs in comparison with the corresponding reference patterns (ICDD no 060311 for CsI, red line). (e) UV-visible absorption (black line) and PL (blue line) spectra of CsI:Zn NCs. Insets in the top right show photographs of NCs solution under room light and UV excitation (365 nm).

distance of 0.323 nm, corresponding to the (110) crystal facet of pure CsBr. SAED patterns (Fig. 5c) of CsI:Zn NCs exhibit the dominant diffraction patterns of the crystal planes of (110), (200) and (211).

In Fig. 5d, XRD patterns of CsI:Zn NCs also show higher angles shift and contractive lattice ($a = b = c = 4.283$ Å, $\alpha = \beta = \gamma = 90°$), as compared to pure CsI (ICDD card no 060311, $a = b = c = 4.296$ Å, $\alpha = \beta = \gamma = 90°$). CsI:Zn NCs hold cubic crystal structure with *Pm3m* space group, which is similar to CsBr:Zn NCs. The EDS mapping (Fig. S14†) shows that CsI:Zn NCs are composed of 45.11% Cs, 53.66% I and 1.23% Zn, which is consistent with XRD result. The excess halide ions can be beneficial to their optical performance.[58] The XPS spectra (Fig. S15†) provide the further confirmation of the presence of

Zn in CsI:Zn NCs by the signal peaks of Zn 2p3/2 level at 1021.9 eV and Zn 2p1/2 level at 1044.7 eV.

In Fig. 5e, the absorption spectrum of CsI:Zn NCs reveals a strong exciton peak at 250 nm derived from the highly ionic lattices of CsI NCs and an obviously broad tail from 250 nm to 550 nm, which is not seen in CsI NCs.[53] In the meantime, PL spectrum shows blue emission peaks centered at 415 nm and 440 nm, similar to that of CsBr:Zn NCs. PLE spectrum and time-resolved PL decay curve of CsI:Zn NCs (Fig. S16†) are measured to study their optoelectrical properties further. PLE spectrum of these NCs exhibits a strong peak at around 386 nm. Time-resolved PL decay curve can also be well fitted by mono-exponential decay function ($R^2 = 0.997$), and the calculated average lifetime of CsI:Zn NCs is 1.50 ns, which indicates a single exciton recombination pathway and fast radiative recombination in both zinc doped cesium halide NCs. The change of PLQY of CsI:Zn NCs over storage time is recorded in Fig. S17.† The trend is similar to that of CsBr:Zn NCs. The highest PLQY of CsI:Zn NCs at 78.95% was achieved after storing for 20 days at ambient condition.

Application of CsBr:Zn NCs in LED

To further investigate the potential applications of zinc doped cesium halide NCs in optoelectronic technology, white CsBr:Zn powder was prepared by evaporating solvent under vacuum environment. CsBr:Zn powder emits a bright blue emission under 365 nm UV light excitation in Fig. 6a, which shows an excellent photoluminescence performance.

A blue LED was fabricated by combining blue emission CsBr:Zn NCs with a 365 nm UV light chip. The photograph of the as-fabricated LED under an operating current of 40 mA is shown in the inset of Fig. 6b. The blue LED has the normalized spectral power at around 440 nm (Fig. 6b), which means that CsBr:Zn NCs maintain their original luminescent properties in blue color.[59] Besides, in a wide range of operating currents from 10 to 100 mA, the device kept the spectra unchanged (Fig. 6c) and exhibited the similar emission (Fig. S18†). Due to the stable luminescent spectra, the output light of the blue LED of CsBr:Zn NCs has a good colour stability. A CIE colour coordinate (0.199, 0.158) of the blue LED can been obtained under the operating current of 100 mA (Fig. 6d). The luminous efficiency of the fabricated blue LED is 0.45 lm W^{-1} under the operating current of 100 mA at room temperature. By using UV light chip, the application of blue-emitting CsBr:Zn NCs has been demonstrated.

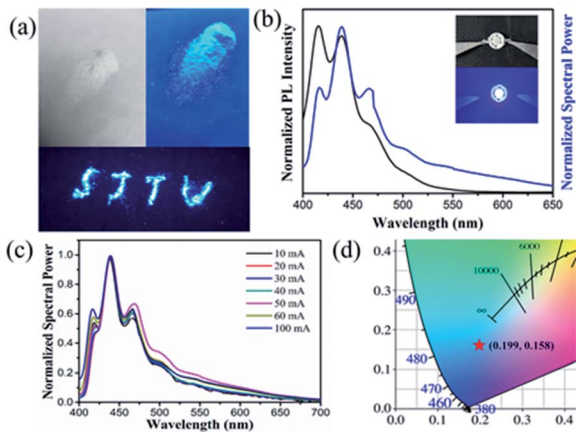

Fig. 6 (a) Photographs of CsBr:Zn NCs powder with and without UV light excitation. (b) Normalized spectral power of the LED fabricated by CsBr:Zn NCs (blue line) and PL spectrum of CsBr:Zn NCs solution (black line). Insets in the top right show photographs of the blue LED in closed and open states. (c) Normalized spectral power of the blue LED under different operating currents from 10 to 100 mA. (d) CIE coordinate corresponding to the blue LED under an operating current of 100 mA.

Conclusions

In summary, we have prepared a series of lead-free and blue luminescent zinc doped cesium halide (CsBr:Zn and CsI:Zn) NCs, outside the family of traditional perovskite halide NCs, *via* a modified hot-injection method. It is interesting to find that the size and shape of the prepared CsBr:Zn NCs change with the storage time under ambient condition, and finally influence the optical properties, especially the PLQY. The prepared CsBr:Zn NCs stored for 30 days with a diameter of 23.3 nm and improved local structure order exhibit the brightest blue emission with a FWHM of 47 nm and PLQY of 79.05%. The high PLQY of CsBr:Zn NCs is among the highest ones for lead-free halide NCs in blue-emitting region as to our knowledge. The CsBr:Zn NCs can be stored under ambient condition for at least 50 days, in which the PLQY still remains 80.67% of the highest PLQY value. CsI:Zn NCs also have a bright blue emission with a high PLQY of 78.95%. The PL spectra of both CsBr:Zn and CsI:Zn NCs are similar. Furthermore, from the observation of temperature dependent PL and narrowing of optical bandgap, zinc doping may induce intermediate trap states in the energy level of cesium halide NCs resulting in bright blue light emission. Multi peaks in PL spectra of both CsBr:Zn and CsI:Zn NCs can also be attributed to multiple intermediate trap states and emissions. Further investigation is still required to understand the photophysical process in the Zn doping. A blue LED fabricated by CsBr:Zn NCs shows stable color spectra and indicates that zinc doped cesium halide NCs are promising candidates for the lighting and display applications.

Conflicts of interest

The authors declare no competing financial interests.

Acknowledgements

This work was partly funded by National Natural Science Foundation of China (Grant No. 51950410581), Shanghai Pujiang Program, and Open Fund of Zhejiang Tsinghua Institute of Flexible Electronics Technology (No. 2019KF2301).

Notes and references

1 Q. Zhao, A. Hazarika, X. Chen, S. P. Harvey, B. W. Larson, G. R. Teeter, J. Liu, T. Song, C. Xiao, L. Shaw, M. Zhang,

G. Li, M. C. Beard and J. M. Luther, *Nat. Commun.*, 2019, **10**, 2842.
2 N. Guijarro, L. Yao, F. Le Formal, R. A. Wells, Y. Liu, B. P. Darwich, L. Navratilova, H. H. Cho, J. H. Yum and K. Sivula, *Angew. Chem., Int. Ed.*, 2019, **58**, 12696–12704.
3 J. Zhang, G. Hodes, Z. Jin and S. F. Liu, *Angew. Chem., Int. Ed.*, 2019, **58**, 15596–15618.
4 X. Wang, L. Wang, T. Shan, S. Leng, H. Zhong, Q. Bao, Z.-H. Lu, L.-L. Deng and C.-C. Chen, *Nano-Micro Lett.*, 2020, **12**, 29–42.
5 L. Wang, X. Wang, L.-L. Deng, S. Leng, X. Guo, C.-H. Tan, W. C. H. Choy and C.-C. Chen, *Mater. Horiz.*, 2020, **7**, 934–942.
6 X. Tang, W. Chen, Z. Liu, J. Du, Z. Yao, Y. Huang, C. Chen, Z. Yang, T. Shi, W. Hu, Z. Zang, Y. Chen and Y. Leng, *Small*, 2019, **15**, e1900484.
7 K. Lin, J. Xing, L. N. Quan, F. P. G. de Arquer, X. Gong, J. Lu, L. Xie, W. Zhao, D. Zhang, C. Yan, W. Li, X. Liu, Y. Lu, J. Kirman, E. H. Sargent, Q. Xiong and Z. Wei, *Nature*, 2018, **562**, 245–248.
8 G. C. Adhikari, S. Thapa, H. Zhu and P. Zhu, *Adv. Opt. Mater.*, 2019, **7**, 1900916.
9 C. Bao, J. Yang, S. Bai, W. Xu, Z. Yan, Q. Xu, J. Liu, W. Zhang and F. Gao, *Adv. Mater.*, 2018, **30**, e1803422.
10 Y. Tang, M. Liang, B. Chang, H. Sun, K. Zheng, T. Pullerits and Q. Chi, *J. Mater. Chem. C*, 2019, **7**, 3369–3374.
11 Y. Dong, Y. Zou, J. Song, X. Song and H. Zeng, *J. Mater. Chem. C*, 2017, **5**, 11369–11394.
12 Q. Zhang, R. Su, X. Liu, J. Xing, T. C. Sum and Q. Xiong, *Adv. Funct. Mater.*, 2016, **26**, 6238–6245.
13 H. Yu, X. Xu, H. Liu, Y. Wan, X. Cheng, J. Chen, Y. Ye and L. Dai, *ACS Nano*, 2020, **14**, 552–558.
14 M. Imran, V. Caligiuri, M. Wang, L. Goldoni, M. Prato, R. Krahne, L. De Trizio and L. Manna, *J. Am. Chem. Soc.*, 2018, **140**, 2656–2664.
15 Z. Xiao, Z. Song and Y. Yan, *Adv. Mater.*, 2019, **31**, e1803792.
16 T. Chiba, S. Ishikawa, J. Sato, Y. Takahashi, H. Ebe, S. Ohisa and J. Kido, *Adv. Opt. Mater.*, 2020, **8**, 2000289.
17 L. Protesescu, S. Yakunin, M. I. Bodnarchuk, F. Krieg, R. Caputo, C. H. Hendon, R. X. Yang, A. Walsh and M. V. Kovalenko, *Nano Lett.*, 2015, **15**, 3692–3696.
18 Q. Fan, G. V. Biesold-McGee, J. Ma, Q. Xu, S. Pan, J. Peng and Z. Lin, *Angew. Chem., Int. Ed.*, 2020, **59**, 1030–1046.
19 J. Sun, J. Yang, J. I. Lee, J. H. Cho and M. S. Kang, *J. Phys. Chem. Lett.*, 2018, **9**, 1573–1583.
20 M. B. Gray, S. Hariyani, T. A. Strom, J. D. Majher, J. Brgoch and P. M. Woodward, *J. Mater. Chem. C*, 2020, **8**, 6797–6803.
21 X. Liu, X. Xu, B. Li, L. Yang, Q. Li, H. Jiang and D. Xu, *Small*, 2020, **16**, e2002547.
22 D. Parobek, B. J. Roman, Y. Dong, H. Jin, E. Lee, M. Sheldon and D. H. Son, *Nano Lett.*, 2016, **16**, 7376–7380.
23 W. J. Mir, M. Jagadeeswararao, S. Das and A. Nag, *ACS Energy Lett.*, 2017, **2**, 537–543.
24 S. Das Adhikari, S. K. Dutta, A. Dutta, A. K. Guria and N. Pradhan, *Angew. Chem., Int. Ed.*, 2017, **56**, 8746–8750.
25 H. Liu, Z. Wu, J. Shao, D. Yao, H. Gao, Y. Liu, W. Yu, H. Zhang and B. Yang, *ACS Nano*, 2017, **11**, 2239–2247.
26 Z. J. Yong, S. Q. Guo, J. P. Ma, J. Y. Zhang, Z. Y. Li, Y. M. Chen, B. B. Zhang, Y. Zhou, J. Shu, J. L. Gu, L. R. Zheng, O. M. Bakr and H. T. Sun, *J. Am. Chem. Soc.*, 2018, **140**, 9942–9951.
27 J.-P. Ma, J.-K. Chen, J. Yin, B.-B. Zhang, Q. Zhao, Y. Kuroiwa, C. Moriyoshi, L. Hu, O. M. Bakr, O. F. Mohammed and H.-T. Sun, *ACS Mater. Lett.*, 2020, **2**, 367–375.
28 P. Yang, G. Liu, B. Liu, X. Liu, Y. Lou, J. Chen and Y. Zhao, *Chem. Commun.*, 2018, **54**, 11638–11641.
29 P. Cheng, L. Sun, L. Feng, S. Yang, Y. Yang, D. Zheng, Y. Zhao, Y. Sang, R. Zhang, D. Wei, W. Deng and K. Han, *Angew. Chem., Int. Ed.*, 2019, **58**, 16087–16091.
30 L. Wang, Z. Shi, Z. Ma, D. Yang, F. Zhang, X. Ji, M. Wang, X. Chen, G. Na, S. Chen, D. Wu, Y. Zhang, X. Li, L. Zhang and C. Shan, *Nano Lett.*, 2020, **20**, 3568–3576.
31 T. C. Jellicoe, J. M. Richter, H. F. Glass, M. Tabachnyk, R. Brady, S. E. Dutton, A. Rao, R. H. Friend, D. Credgington, N. C. Greenham and M. L. Bohm, *J. Am. Chem. Soc.*, 2016, **138**, 2941–2944.
32 A. Wang, Y. Guo, F. Muhammad and Z. Deng, *Chem. Mater.*, 2017, **29**, 6493–6501.
33 A. B. Wong, Y. Bekenstein, J. Kang, C. S. Kley, D. Kim, N. A. Gibson, D. Zhang, Y. Yu, S. R. Leone, L.-W. Wang, A. P. Alivisatos and P. Yang, *Nano Lett.*, 2018, **18**, 2060–2066.
34 A. Wang, X. Yan, M. Zhang, S. Sun, M. Yang, W. Shen, X. Pan, P. Wang and Z. Deng, *Chem. Mater.*, 2016, **28**, 8132–8140.
35 D. S. Dolzhnikov, C. Wang, Y. Xu, M. G. Kanatzidis and E. A. Weiss, *Chem. Mater.*, 2017, **29**, 7901–7907.
36 Z. Tan, J. Li, C. Zhang, Z. Li, Q. Hu, Z. Xiao, T. Kamiya, H. Hosono, G. Niu, E. Lifshitz, Y. Cheng and J. Tang, *Adv. Funct. Mater.*, 2018, **28**, 1801131.
37 J. Huang, T. Lei, M. Siron, Y. Zhang, S. Yu, F. Seeler, A. Dehestani, L. N. Quan, K. Schierle-Arndt and P. Yang, *Nano Lett.*, 2020, **20**, 3734–3739.
38 B. Yang, J. Chen, F. Hong, X. Mao, K. Zheng, S. Yang, Y. Li, T. Pullerits, W. Deng and K. Han, *Angew. Chem., Int. Ed.*, 2017, **56**, 12471–12475.
39 B. Yang, J. Chen, S. Yang, F. Hong, L. Sun, P. Han, T. Pullerits, W. Deng and K. Han, *Angew. Chem., Int. Ed.*, 2018, **57**, 5359–5363.
40 B. Yang, X. Mao, F. Hong, W. Meng, Y. Tang, X. Xia, S. Yang, W. Deng and K. Han, *J. Am. Chem. Soc.*, 2018, **140**, 17001–17006.
41 L. Zhou, Y. F. Xu, B. X. Chen, D. B. Kuang and C. Y. Su, *Small*, 2018, **14**, e1703762.
42 D. Zhu, M. L. Zaffalon, V. Pinchetti, R. Brescia, F. Moro, M. Fasoli, M. Fanciulli, A. Tang, I. Infante, L. De Trizio, S. Brovelli and L. Manna, *Chem. Mater.*, 2020, **32**, 5897–5903.
43 P. Cheng, L. Feng, Y. Liu, D. Zheng, Y. Sang, W. Zhao, Y. Yang, S. Yang, G. Wang and K. Han, *Angew. Chem., Int. Ed.*, 2020, **132**, 1–6.
44 H. Shankar, S. Ghosh and P. Kar, *J. Alloys Compd.*, 2020, **844**, 156148.
45 M. Cardona, R. Haensel, D. W. Lynch and B. Sonntag, *Phys. Rev. B*, 1970, **2**, 1117–1131.
46 J. R. Maldonado, S. T. Coyle, B. Shamoun, M. Yu, M. Gesley and P. Pianetta, *J. Vac. Sci. Technol., B*, 2004, **22**, 3025–3031.

47 V. V. Nagarkar, C. Brecher, E. E. Ovechkina, V. Gaysinskiy, S. R. Miller, S. Thacker, A. Lempicki and R. H. Bartram, *IEEE Trans. Nucl. Sci.*, 2008, **55**, 1270–1274.
48 M. Nikl and A. Yoshikawa, *Adv. Opt. Mater.*, 2015, **3**, 463–481.
49 Z. Yang, Z. Jiang, X. Liu, X. Zhou, J. Zhang and W. Li, *Adv. Opt. Mater.*, 2019, **7**, 1900108.
50 S. Hou, M. K. Gangishetty, Q. Quan and D. N. Congreve, *Joule*, 2018, **2**, 2421–2433.
51 F. Yuan, Y.-K. Wang, G. Sharma, Y. Dong, X. Zheng, P. Li, A. Johnston, G. Bappi, J. Z. Fan, H. Kung, B. Chen, M. I. Saidaminov, K. Singh, O. Voznyy, O. M. Bakr, Z.-H. Lu and E. H. Sargent, *Nat. Photonics*, 2019, **14**, 171–176.
52 H. Shen, Q. Gao, Y. Zhang, Y. Lin, Q. Lin, Z. Li, L. Chen, Z. Zeng, X. Li, Y. Jia, S. Wang, Z. Du, L. S. Li and Z. Zhang, *Nat. Photonics*, 2019, **13**, 192–197.
53 J. Shamsi, Z. Dang, P. Ijaz, A. L. Abdelhady, G. Bertoni, I. Moreels and L. Manna, *Chem. Mater.*, 2018, **30**, 79–83.
54 X. Shen, Y. Zhang, S. V. Kershaw, T. Li, C. Wang, X. Zhang, W. Wang, D. Li, Y. Wang, M. Lu, L. Zhang, C. Sun, D. Zhao, G. Qin, X. Bai, W. W. Yu and A. L. Rogach, *Nano Lett.*, 2019, **19**, 1552–1559.
55 H. Sun, J. Zhang, X. Gan, L. Yu, H. Yuan, M. Shang, C. Lu, D. Hou, Z. Hu, Y. Zhu and L. Han, *Adv. Energy Mater.*, 2019, **9**, 1900896.
56 J. Y. Woo, Y. Kim, J. Bae, T. G. Kim, J. W. Kim, D. C. Lee and S. Jeong, *Chem. Mater.*, 2017, **29**, 7088–7092.
57 J. Song, T. Fang, J. Li, L. Xu, F. Zhang, B. Han, Q. Shan and H. Zeng, *Adv. Mater.*, 2018, **30**, 1805409.
58 J. Zhang, Y. Yang, H. Deng, U. Farooq, X. Yang, J. Khan, J. Tang and H. Song, *ACS Nano*, 2017, **11**, 9294–9302.
59 Y. Shen, J. Yin, B. Cai, Z. Wang, Y. Dong, X. Xu and H. Zeng, *Nanoscale Horiz.*, 2020, **5**, 580–585.
60 B. Yang, L. Yin, G. Niu, J. H. Yuan, K. H. Xue, Z. Tan, X. S. Miao, M. Niu, X. Du and H. Song, *Adv. Mater.*, 2019, **31**, 1904711.
61 J. Luo, X. Wang, S. Li, J. Liu, Y. Guo, G. Niu, L. Yao, Y. Fu, L. Gao, Q. Dong, C. Zhao, M. Leng, F. Ma, W. Liang, L. Wang, S. Jin, J. Han, L. Zhang, J. Etheridge, J. Wang, Y. Yan, E. H. Sargent and J. Tang, *Nature*, 2018, **563**, 541–545.
62 S. Kahmann, O. Nazarenko, S. Shao, O. Hordiichuk, M. Kepenekian, J. Even, M. V. Kovalenko, G. R. Blake and M. A. Loi, *ACS Energy Lett.*, 2020, **5**, 2512–2519.
63 S. Jana, S. Mukherjee, A. Ghorai, S. B. N. Bhaktha and S. K. Ray, *Adv. Opt. Mater.*, 2020, **8**, 2000180.
64 N. Mondal, A. De and A. Samanta, *ACS Energy Lett.*, 2018, **4**, 32–39.
65 A. Karmakar, M. S. Dodd, S. Agnihotri, E. Ravera and V. K. Michaelis, *Chem. Mater.*, 2018, **30**, 8280–8290.
66 R. Aceves, V. Babin, M. B. Flores, P. Fabeni, E. Mihokova, M. Nikl, K. Nitsch, G. P. Pazzi, R. P. Salas, N. Zazubovich and S. Zazubovich, *Phys. Status Solidi B*, 2001, **223**, 745–756.
67 Q. Liao, J. Chen, L. Zhou, T. Wei, L. Zhang, D. Chen, F. Huang, Q. Pang and J. Z. Zhang, *J. Phys. Chem. Lett.*, 2020, **11**, 8392–8398.
68 C. Lushchik, R. Gindina, S. Zazubovich and N. Lushchik, *Czechoslovak Czech. J. Phys.*, 1970, **20**, 585–604.
69 P. B. Fitzsimons and J. Corish, *Phys. Status Solidi*, 1985, **91**, 543–548.
70 P. Hackenschmied, G. Schierning, M. Batentschuk and A. Winnacker, *J. Appl. Phys.*, 2003, **93**, 5109–5112.